An Ultra-Wideband Microwave Radar Sensor for Characterizing Pavement Subsurface

Joongsuk Park and Cam Nguyen

Department of Electrical Engineering, Texas A&M University, College Station, TX 77843-3128

Abstract — A new ultra-wideband (UWB) stepped-frequency radar sensor operating from 0.6 to 5.6 GHz has been developed using microwave integrated circuits for pavement subsurface characterization. UWB microstrip quasi-horn antennas have also been designed and tested for use in the sensor. A new simple yet effective, accurate procedure was developed to compensate the amplitude deviations and non-linear phase errors of the complex I/Q vectors due to the inherent imperfection of the system. The system has been used to assess a pavement sample with good accuracy.

I. INTRODUCTION

Microwave sensing has been proven as a valuable technique for characterizing subsurface. Microwave step-frequency radar (SFR) can provide both deep penetration and fine resolution simultaneously for subsurface sensing and is, thus, attractive for subsurface evaluation such as measuring layer thickness and detecting damages in pavement structures.

Most of the reported microwave SFR's for subsurface applications operate at low frequencies and have narrow bandwidths. For example, a SFR, developed for detection of water below the pavement surface, operates from 600 MHz to 1.112 GHz [1]. Another SFR operating from 490 to 780 MHz was developed for detection of buried objects [2]. Recently, a HP network analyzer operating from 0.5 to 6 GHz was also used as a SFR to detect concrete cracks [3]. There is no SFR, completely realized using microwave integrated circuits (MICs) and operated over a decade of frequency bandwidth, has been reported for subsurface sensing.

In this paper, we report for the first time a new compact UWB microwave SFR sensor operating from 0.6 to 5.6 GHz for measuring subsurface characteristics of pavement. The sensor is implemented using a coherent super-heterodyne scheme and completely realized using MICs. It employs two UWB microstrip quasi-horn antennas operating from 0.5 GHz to more than 10 GHz. Its performance has been demonstrated through accurate measurements of pavement subsurface.

II. SYSTEM PRINCIPLE

SFR sensor transmits sequences of N sinusoidal signals of different frequencies toward a target, receives return signals from the target, and processes the return signals for target characteristics. In each sequence, the frequency is shifted in discrete values – each value is held constant for a period of time and then changed to a next higher value [4].

The received signals at step frequencies, reflected from the target, are down-converted into an intermediate-frequency (IF) signal. This IF signal is then demodulated into in-phase (I) and quadrature-phase (Q) signals in base band. The I/Q signals represent both the amplitude and phase information of the targets. Upon converting these analog I/Q signals into digital I/Q samples, digital signal processing is applied on the I/Q samples to retrieve a representative complex vector at each frequency. Each set of N samples are combined to form a complex vector array, $I + jQ$, from which a time domain synthetic pulse representing the target is extracted and processed to reveal the pavement's subsurface characteristics.

III. SYSTEM DESIGN AND MEASUREMENT

Fig. 1 shows the system configuration of the newly developed UWB microwave SFR sensor based on a coherent super-heterodyne architecture. The sensor consists of transceiver, two antennas and digital signal processing.

A. Transceiver

The temperature compensated crystal oscillator (TCXO) in the transceiver generates a signal of 10 MHz, which is used as the LO signal for the quadrature demodulator and the IF signal for the up-

0-7803-7695-1/03/$17.00 © 2003 IEEE

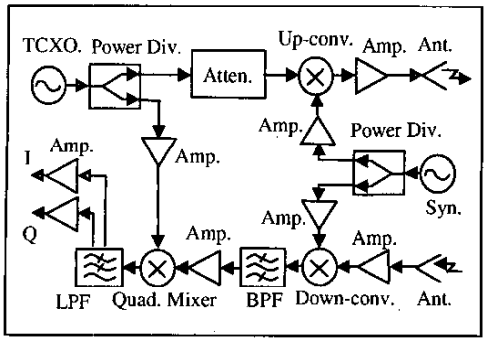

Fig. 1. Block diagram of the UWB SFR sensor.

converter. The up-converter converts the incoming 0.6-5.6-GHz LO signals from the synthesizer to 0.61-5.61-GHz signals, which are transmitted toward the targets (through an UWB transmit antenna.) The return signals from the targets (through the receive antenna) are down-converted to an IF signal of 10 MHz by mixing with the coherent LO signals from the synthesizer in the down-converter. The IF signal is then converted into the base-band I/Q signals by mixing with the coherent LO signal from the TCXO in the quadrature demodulator. The I/Q signals are finally digitized in an analog-to-digital converter (ADC) and used to extract the subsurface characteristics.

Imperfection of the system causes amplitude deviations and non-linear phase errors of the base band I/Q vectors. To offset this problem, we employ a new compensation technique, which is simple yet effective and accurate. Complex vectors, I+jQ, are measured when a metal plate is moved along a track at a fixed frequency. Initially, the complex vector rotates elliptically, either clockwise or counter-clockwise, with respect to the direction of the metal plate, as the I and Q components are not orthogonal due to the phase errors. However, after the errors are corrected, the I and Q components become orthogonal and the complex vector starts rotating circularly. The amplitude level and the non-linear phase error at the fixed frequency are then stored as references. This procedure is repeated at each frequency step across the operating frequency range.

Fig. 2 shows the measured vectors' amplitude deviations and non-linear phase errors, used for correction, in the band of interest.

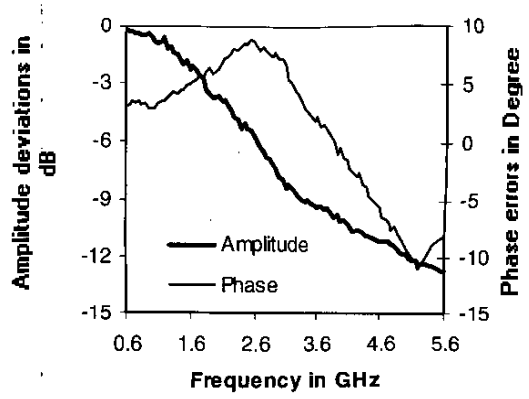

Fig. 2. Amplitude deviations and non-linear phase errors of the complex vectors due to the imperfection of the system.

B. Antenna

TEM horn antennas are commonly used for UWB radars owing to their inherent characteristics of wide bandwidth, high directivity, good phase linearity, and low distortion. Various types of TEM horn antennas have been developed [5]-[7]. A TEM horn antenna, however, needs balun at its input. Hence, integrating these antennas directly with the transceiver circuit is not suitable. In addition, direct coupling between the transmitting and receiving antennas in a bi-static system is inevitable.

Novel microstrip quasi-horn antennas (Fig. 3) are employed in our system to allow a direct integration with the transceiver while maintaining adequate isolation between the two antennas.

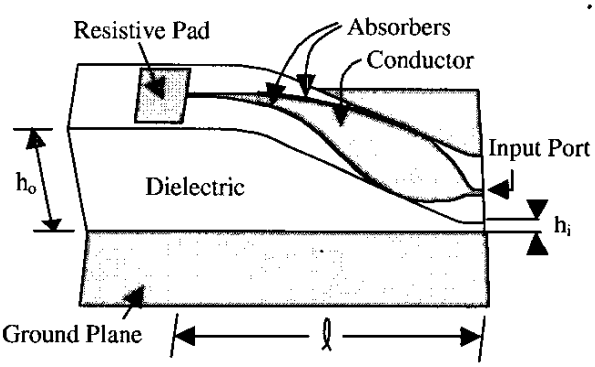

Fig. 3. UWB microstrip quasi-horn antenna.

The antenna was designed to present at least 10 dB of return loss over a wide band of 0.5-10 GHz. The

length of the antenna, which is primarily restricted by the lowest operating frequency, is set to 16 inches. Reflections from the open end and the edges were significantly reduced by appending a resistive pad to the open end and absorbers to the edges. This is illustrated in Fig. 3. The resistive pad, which is made of a metal film with thickness of 0.025 inch and 250 ohms/square, was tuned empirically to an optimal size of 2x3 inches. Computer simulations were performed using Ansoft's HFSS program to theoretically verify the reflection coefficients and the far field radiation patterns.

Fig. 4 shows the measured reflection coefficients in both the time and frequency domains. The reflection coefficient at the low frequency end, as seen in the frequency-domain plot, is improved significantly due to the incorporation of the resistive pad and absorbers. A better illustration of the impact of these accessories is shown in the time domain plots. An additional narrow peak, indicating deterioration of the input reflection coefficient, is observed at around 3.5 ns when the resistive pad and absorbers were not incorporated.

C. Digital Signal Processing

Using coherent demodulation, analog samples over a period of interest are first obtained. A sampling frequency that is much higher than the switching frequency of the synthesizer is then used to sample the analog I/Q signals. The samples are then synchronized, restored, filtered and averaged to obtain a representative data point (Fig. 5). The settling time, ζ, of a synthesizer and the delayed time, τ, of the received signals should be considered since non-coherent demodulation occurs during the time $\zeta + \tau$. The samples are useless during the time $\zeta + \tau$, and it is thus necessary to restore the samples with only effective samples as shown in Fig. 5. The samples at each packet, C_{k1}, C_{k2}, ..., C_{km} where C_{km} denotes the m^{th} complex vector corresponding to the k^{th} frequency, are filtered and averaged to generate a new complex vector, C_k, as shown in Fig. 5(d). Averaging the samples reduces the errors caused by short time jitters of the TCXO and the synthesizer.

In order to reduce the effects of imperfection of the system, a compensation procedure utilizing the stored reference data described earlier, is used. After synchronizing, restoring, filtering and averaging the measured I/Q signals, the newly generated complex

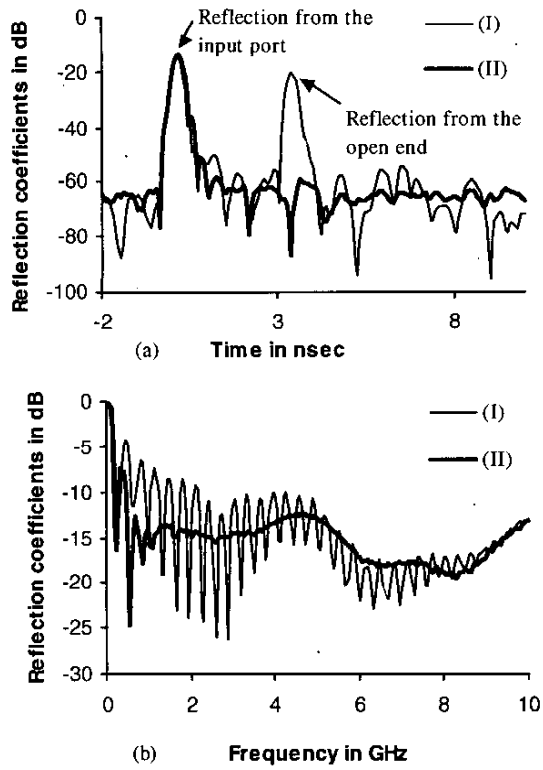

Fig. 4. Antenna's reflection coefficient. Time domain (a), Frequency domain (b) where (I) indicates the antenna alone and (II) represents the antenna with a resistive pad and absorbers.

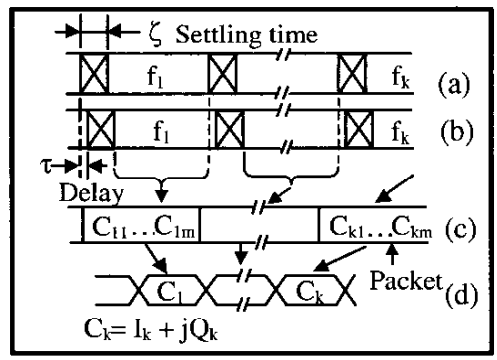

Fig. 5. Procedure for generating representative complex vectors: (a) transmitted signals, (b) received signals, (c) restored effective complex vectors, (d) representative complex vectors after averaging.

vector is compensated by using amplitude deviations and phase errors in the memory. Note that the amplitude deviation at each frequency step is normalized before multiplying it with the complex vector needed for compensation.

Zero padding is needed to improve the accuracy of the range and the speed of IDFT. An appropriate window function is used to reduce the side-lobes of the synthetic pulses, which might mask other pluses caused by multiple targets. The synthetic pulses are then used to determine parameters of the subsurface layers of the pavement.

D. Measurements

A pavement sample was constructed with two layers in a wooden box of 36 in.x36 in.. The top layer is asphalt having a thickness of 2.6-2.7 inches. The bottom layer is base. It has a thickness of 4.1 inches and is filled with limestone. The sensor's antennas were pointed directly onto the sample, without contact, through air. Table I shows the measured parameters of the pavement sample along with the actual values. The measured thickness of each layer agrees well with the actual value. Note that the theoretical relative permittivities of the sample's asphalt and base materials are not known. Several values of relative permittivity for asphalt and base can be found from literature but these are not used for comparison here since 1) the reported values vary over a wide range, 2) they are at frequencies different from those used here and 3) the reported asphalt and base materials are not the same as those in our pavement sample.

TABLE I

Comparison between actual and measured data

		Asphalt	Base
Relative Permittivity	Experiment	3.24	12.5
Thickness (inches)	Actual	2.6-2.7	4.1
	Experiment	2.72	4.04

IV. CONCLUSION

A new integrated-circuit UWB microwave SFR sensor including antennas has been successfully developed and demonstrated for accurate measurement of pavement subsurface. A new correction procedure was also developed for compensating the imperfection of the system. Its operation has been verified by measuring layer thickness and relative dielectric constant of a pavement sample. The system represents the first 0.6-5.6-GHz portable microwave SFR developed for pavement subsurface sensing and is useful not only for non-destructive evaluation of pavements and other highway structures, but also for other subsurface sensing applications like detection of buried mines.

ACKNOWLEDGEMENT

This work was supported in part by the National Science Foundation and in part by the National Academy of Sciences. The authors wish to thank to Tom Scullion and Lee Gustavus of Texas Transport Institute for providing the pavement sample.

REFERENCES

[1] R. C. Pippert, K. Soroushian, and R. G. Plumb, "Development of a Ground-Penetrating Radar to Detect Excess Moisture in Pavement Subgrade," *Proceedings of the Second Government Workshop on GPR – Advanced Ground Penetrating Radar: Technologies and Applications,* pp. 283-297, Oct. 1993.

[2] A. Langman, S. P. Dimaio, B. E. Burns, and M. R. Inggs, "Development of a Low Cost SFCW Ground Penetrating Radar," *IEEE Geoscience and Remote Sensing Symposium,* pp. 2020-2022, 1996.

[3] D. Huston, J. O. Hu, K. Maser, W. Weedon, and C. Adam, "GIMA Ground Penetrating Radar System for Monitoring Concrete Bridge Decks, " *Journal of Applied Geophysics,* vol. 43, pp. 139-146, 2000.

[4] D. R. Wehner, *High Resolution Radar*, Artech House, 1995.

[5] E. A. Theodorou, M. R. Gorman, P. R. Rigg, and F. N. Kong, "Broadband pulse-optimized antenna," *Proc. Inst. Elec.,* vol. 128, pt. H, pp. 124-130, June 1981

[6] J. D. Cermignani, R. G. Madonna, P. J. Scheno, and J. Anderson, "Measurement of the Performance of A Cavity Backed Exponentially Flared TEM Horn, " *SPIE, Ultrawideband Radar,* vol. 1631, pp. 146-154, 1992.

[7] M Kanda, "The effects of resistive loading of "TEM" horns," *IEEE Trans. Electromag. Comp.,* vol. 24, pp. 245-255, May 1982.